Numerical study of the force network ensemble

A. R. T. van Eerd[a]; B. P. Tighe[b]; T. J. H. Vlugt[c]

[a] Condensed Matter and Interfaces, Department of Chemistry, Utrecht University, Utrecht, The Netherlands [b] Instituut-Lorentz, Leiden University, Leiden, The Netherlands [c] Process and Energy Laboratory, Delft University of Technology, Delft, The Netherlands

PLEASE SCROLL DOWN FOR ARTICLE

Taylor & Francis
Taylor & Francis Group

Numerical study of the force network ensemble

A.R.T. van Eerd[a], B.P. Tighe[b] and T.J.H. Vlugt[c]*

[a]*Condensed Matter and Interfaces, Department of Chemistry, Utrecht University, P.O. Box 80.000, 3508 TA, Utrecht, The Netherlands;*
[b]*Instituut-Lorentz, Leiden University, P.O. Box 9506, 2300 RA, Leiden, The Netherlands;* [c]*Process and Energy Laboratory, Delft University of Technology, Leeghwaterstraat 44, 2628 CA Delft, The Netherlands*

The force network ensemble of Snoeijer et al. (*Force network ensemble: a new approach to static granular matter*, Phys. Rev. Lett. 92 (2004), 054302) is a convenient model to study networks of contact forces that are typically present in granular matter. Recently, we have shown that it is possible to extremely accurately determine the probability distribution of contact forces in the framework of this ensemble (van Eerd et al., *Tail of the contact force distribution in static granular materials*, Phys. Rev. E 75 (2007), 060302(R); Tighe et al., *Entropy maximisation in the force network ensemble for granular solids*, Phys. Rev. Lett. 100 (2008), 238001). In this work, we review several important details of these computations. In particular, we study in detail the angle-resolved contact force distribution, finite-size effects, the maximum allowed shear stress and the effect of walls. In addition, we investigate how well the force network ensemble resembles systems with 'real' interactions.

Keywords: granular materials; force network ensemble; Monte Carlo simulation

1. Introduction

Granular materials are systems consisting of a large number of interacting macroscopic particles, such as sand, rice or apples. For these systems, the range of the interaction is short compared to the particle size and Brownian motion does not play a role. Granular materials are important in everyday life. A good understanding of the physics of granular materials is desired, for example, to predict and control landslides and avalanches [1,2], to design efficient transport and handling of coal or chemicals [3,4] and to make high-quality tablets (medicine), i.e. the correct amounts of active and inert ingredients [5,6]. Unfortunately, there still remains a poor understanding of the behaviour of granular matter [7–9].

Contact forces in granular materials are organised into very heterogeneous force networks, and it is generally accepted that a detailed understanding of the statistics of the contact forces is required for understanding the behaviour of these materials [10]. A convenient way to study and characterise force networks is by means of the probability distribution of contact forces, $P(f)$. This has been the topic of many experimental [11–16], theoretical [17–22] and computer simulation studies [23–27].

The force network ensemble is a recently introduced statistical formulation to study the statistics of contact forces in static granular media [28,29]. The crucial assumption is that for fixed particle positions, all force configurations of non-cohesive contact forces that result in force- and torque balance on all particles are equally likely. This approach can be regarded as a restricted version of the Edwards ensemble [30]. For several regular

and disordered packings the contact force distribution $P(f)$ was calculated [28,29], which had all the features that were typically observed in experiments and numerics, and subsequently the force network ensemble has received a lot of attention [31–38]. Recently, using umbrella sampling simulations, we unambiguously showed that in the force network ensemble the distribution of contact forces between particles shows a *Gaussian* decay for large contact forces [39], in sharp contrast to the general belief that *exponential* force statistics is a characteristic feature of granular matter. It turns out that the Gaussian decay is a direct result of the local force balance on particles [40].

In the present paper, we will use numerical simulations to study several important aspects of the force network ensemble more in detail. In particular, we focus on the details of stress constraints and finite-size effects for the frictionless triangular lattice (Section 3.1), the angle-resolved contact force distribution (Section 3.2), finite-size effects and the maximum possible contact force of a certain network of contact forces (Section 3.3), the maximum shear stress of a packing (Section 3.4) and the effect of walls (Section 3.5). Finally, in Section 3.6, we will investigate a crucial and longstanding question: how well does the force network ensemble describe systems with 'real' inter-actions? We summarise our findings in Section 4.

2. Model and simulation method

In the force network ensemble it is assumed that a separation of length scales between the contact forces and the positions

occur. Therefore, one can treat the forces as independent from the positions [30]. In this way, one can construct an ensemble in which the positions of all the particles are fixed, and the non-cohesive contact forces are the degrees of freedom that have to satisfy the force- and torque balance on each particle. For a fixed packing geometry of frictionless particles, the net force $\mathbf{F}_i$ on each particle i is zero

$$\mathbf{F}_i = \sum_j \mathbf{f}_{ij} = \sum_j f_{ij} \frac{\mathbf{r}_{ij}}{|\mathbf{r}_{ij}|} = 0, \tag{1}$$

in which j runs over the particles in contact with particle i and $\mathbf{r}_{ij} = \mathbf{r}_i - \mathbf{r}_j$. Consider a d-dimensional system with N particles and periodic boundary conditions. To describe mechanical equilibrium in d directions, $dN - d$ linear constraints are needed. If frictional particles are considered, then N (for 2D) or $3N$ (for 3D) additional constraints are needed to obtain torque balance on each particle. In addition to the force balance constraints, it is necessary to constrain the applied stress on the system. The applied stress on a system is defined by the stress tensor

$$\boldsymbol{\sigma} = \begin{pmatrix} \sigma_{xx} & \sigma_{xy} \\ \sigma_{yx} & \sigma_{yy} \end{pmatrix} \text{ in 2D, and } \boldsymbol{\sigma} = \begin{pmatrix} \sigma_{xx} & \sigma_{xy} & \sigma_{xz} \\ \sigma_{yx} & \sigma_{yy} & \sigma_{yz} \\ \sigma_{zx} & \sigma_{zy} & \sigma_{zz} \end{pmatrix} \text{ in 3D} \tag{2}$$

in which

$$\sigma_{\alpha\beta} = \frac{1}{N_b} \sum_{ij} f_{ij,\alpha} r_{ij,\beta}. \tag{3}$$

In this equation, $N_b = zN/2$ equals the total number of contacts. In 2D, the contact force in directions α and $f_{ij,\alpha}$ can be written as

$$f_{ij,x} = f_{n,ij} \frac{r_{ij,x}}{|\mathbf{r}_{ij}|} + f_{t,ij} \frac{r_{ij,y}}{|\mathbf{r}_{ij}|}, \tag{4}$$

$$f_{ij,y} = f_{n,ij} \frac{r_{ij,y}}{|\mathbf{r}_{ij}|} - f_{t,ij} \frac{r_{ij,x}}{|\mathbf{r}_{ij}|} \tag{5}$$

in which $f_{n,ij}$ and $f_{t,ij}$ are the normal and tangential components of the contact force, respectively. The dimensionless shear stress is defined as $\tau = \sigma_{\alpha\beta}/\sigma_{\alpha\alpha}$ and the pressure on the system is proportional to $\sum_\alpha \sigma_{\alpha\alpha}$.

An isotropic pressure corresponds to $\sigma_{xx} = \sigma_{yy} (= \sigma_{zz})$. By imposing $\langle f \rangle = 1$ a force scale is introduced. This was used in all the simulations described in this work. Substituting Equations (4) and (5) in (3), we find $\sigma_{\alpha\alpha} = 1/d$ in the case that $|\mathbf{r}_{ij}| = 1$ (monodisperse particles).

It is convenient to represent the collection of all the contact forces in the system ($f_{n,ij}$ and $f_{t,ij}$) by the vector $\mathbf{f}$. The elements of $\mathbf{f}$ are subject to the constraints that all the particles have force and torque balance, all the contact forces are repulsive and that the constraints on the stress tensor are satisfied. In Table 1, the number of constraints and the number of elements of $\mathbf{f}$ are summarised. For packings with a contact number z larger than the critical contact number z_c ($z_c = 4$ for frictionless and $z_c = 3$ for frictional 2D packings, respectively [28]), the number of elements of $\mathbf{f}$ exceeds the number of constraints, which means that there is a high-dimensional force space of solutions. Note that in dry granular media all contact forces are repulsive, which is incorporated by demanding all normal forces f_n to be positive

$$f_{n,ij} \geq 0. \tag{6}$$

For frictional packings, the magnitude of the tangential force is bound by the Coulomb criterion

$$|f_{t,ij}| \leq \mu f_{n,ij}, \tag{7}$$

μ being the friction coefficient. Snoeijer et al. assumed that all the allowed solutions of this force space are equally likely, as in the microcanonical ensemble and the Edwards ensemble [30]. The corresponding ensemble is therefore called the *force network ensemble*. Using the force network ensemble with this flat measure, realistic contact force distributions have been obtained, both for triangular lattices and disordered packings [28].

Snoeijer et al. [29] obtained analytical solutions for $P(f)$ in the force network ensemble for various small systems: 'snooker' packings [41] of three and six particles, periodic triangular lattices of 2×2 and 3×3, and a periodic fcc unit cell (eight particles). Tighe et al. [32] derived the analytical expressions for both isotropic and anisotropic force distributions in the 3×3 triangular lattice. However, it was found that these analytical approaches are not usable for larger packings. Therefore, we have to rely on computer simulations for these systems.

Table 1. The number of constraints (force and torque balance on each particle, fixed stress tensor $\boldsymbol{\sigma}$) and the number of elements of $\mathbf{f}$ for systems with periodic boundary conditions, N particles and an average coordination number z in the force network ensemble.

Dimension d	Friction	Number of constraints	Number of elements of $\mathbf{f}$
2	No	$2N - 2 + 3$	$zN/2$
2	Yes	$2N - 2 + 3 + N$	zN
3	No	$3N - 3 + 6$	$zN/2$
3	Yes	$3N - 3 + 6 + 3N$	zN

To compute a *single* solution for the force space, a simulated annealing procedure can be applied [42]. For arbitrary contact forces, a penalty function $U(\mathbf{f})$ is defined that describes the deviation from the required constraints. For a 2D frictionless system with $|\mathbf{r}_{ij}| = 1$, this penalty function is defined as

$$U(\mathbf{f}) = \left| \sigma_{xy}(\mathbf{f}) - \sigma_{xy}^{\text{req}} \right| + \left| \sigma_{xx}(\mathbf{f}) - \frac{1}{2} \right| + \left| \sigma_{yy}(\mathbf{f}) - \frac{1}{2} \right|$$
$$+ \sum_{i=1}^{N} |F_{i,x}(\mathbf{f})| + \sum_{i=1}^{N} |F_{i,y}(\mathbf{f})| \qquad (8)$$

in which σ_{xy}^{req} is the required (imposed) shear stress of the system. The following Monte Carlo procedure can be used to generate a *single* force network $\mathbf{f}$ that obeys the required constraints.

(1) Start with a configuration $\mathbf{f}_{\text{old}}$ in which all contact forces are taken from an arbitrary distribution with $\langle f \rangle = 1$ and $f_{\text{n},ij} \geq 0$. Set the control parameter $\beta = 1$ (equivalent to the inverse temperature) and calculate the penalty function $U(\mathbf{f}_{\text{old}})$.
(2) Select two elements (contact forces) of $\mathbf{f}$ at random.
(3) Add a randomly selected Δf to one contact force and $-\Delta f$ to the other contact force, so that $\langle f \rangle$ still equals 1. If any of these (normal) forces become smaller than 0, the move is rejected and we return to step 2.
(4) Calculate the penalty function $U(\mathbf{f}_{\text{new}})$.
(5) Accept the trial move with the usual Metropolis acceptance rule [43]. If rejected, the old configuration is kept.
(6) Increase β by multiplying with a factor $h > 1$ (i.e. annealing).
(7) Return to step 2 if the penalty function is very small (typically $U(\mathbf{f})/N < 10^{-12}$). The resulting $\mathbf{f}$ is considered as a particular solution of the force network ensemble.

It is trivial to extend this scheme for frictional packings and packings with $|\mathbf{r}_{ij}| \neq 1$. In previous studies [28,29,35,44], the solution space of the force network ensemble was sampled by generating many particular solutions obtained using this simulated annealing scheme. This scheme reproduces analytic results for small regular packings very well [29] and it was verified that the results do not depend on the initial configuration and details of the annealing scheme. Unfortunately, this simulated annealing procedure is computationally expensive and it cannot be guaranteed that force networks are indeed generated with equal *a priori* probability. Moreover, accurate statistics for large contact forces cannot be obtained directly.

At this point, it is important to note that the force network ensemble can be formulated as an inhomogeneous matrix equation

$$\mathcal{A}\mathbf{f} = \mathbf{b}, \qquad (9)$$

in which the static force (and torque) balance on each particle as well as a conserved stress tensor are incorporated. All possible solutions of this matrix equation can be written as

$$\mathbf{f} = \mathbf{f}_0 + \sum_k a_k \mathbf{v}_k, \qquad (10)$$

where $\mathbf{f}_0$ is a *particular* solution and the vectors $\mathbf{v}_k$ span the null-space of matrix $\mathcal{A}$, i.e.

$$\mathcal{A}\mathbf{v}_k = 0. \qquad (11)$$

The number of independent null vectors is listed in Table 1. The force network ensemble is sampled by the usual Metropolis Monte Carlo technique [45] in which the coefficient a_k is the degree of freedom. The Monte Carlo scheme starts with $a_k = 0$ and a particular solution $\mathbf{f}_0$. In a trial move, a coefficient a_k is chosen at random and its value is changed randomly. A trial move is accepted when all normal forces are $f_{\text{n},ij} \geq 0$, and rejected if otherwise. For frictional systems, one has to take into account the Coulomb friction law (Equation (7)) in the acceptance rule. For the triangular, square and fcc lattice, it is convenient to choose $\mathbf{f}_0$ such that all elements $\mathbf{f}_0$ are all equal to 1. The null-space $\mathbf{v}_k$ of these systems can be expressed by the so-called 'wheel moves' developed by Tighe et al. [32].

To improve the statistics of large contact forces, we employ the umbrella sampling technique [45,46]. Each realisation of the force network $\mathbf{f}$ is characterised by the largest contact force f_{max}. The Monte Carlo simulations are performed in a modified ensemble with a modified probability density

$$\rho_{\pi}(\mathbf{f}) = \rho(\mathbf{f}) \exp\left[W(f_{\text{max}}(\mathbf{f}))\right] \qquad (12)$$

in which $\rho(\mathbf{f})$ is the probability density in the force network ensemble and $W(f_{\text{max}})$ is the arbitrary weight function. The probability distributions of f_{max} in the original and modified ensemble (denoted by π) are related by

$$P(f_{\text{max}}) \propto P_{\pi}(f_{\text{max}}) \exp\left[-W(f_{\text{max}})\right]. \qquad (13)$$

In general, the ensemble average of a certain quantity A in the original force network ensemble can be recovered by appropriate reweighing

$$\langle A \rangle = \frac{\langle A(\mathbf{f}) \exp\left[-W(f_{\text{max}}(\mathbf{f}))\right] \rangle_{\pi}}{\langle \exp\left[-W(f_{\text{max}}(\mathbf{f}))\right] \rangle_{\pi}}, \qquad (14)$$

in which we used the shorthand $\langle \cdots \rangle_{\pi}$ for averages in the modified ensemble. To ensure that large contact forces are adequately sampled, we chose the function $W(f_{\text{max}})$ such

that the probability distribution of f_{max} in the modified ensemble ($P_\pi(f_{max})$) is approximately flat, so that $W(f_{max}) = -\ln P(f_{max})$. For more details of this scheme, we refer the reader to [47].

3. Results and discussion

3.1 Details of the stress constraints and finite-size effects

In the force network ensemble, it is natural to introduce a force scale by imposing $\langle f \rangle = 1$. In the case of a monodisperse system (i.e. $|\mathbf{r}_{ij}| = 1$), this directly results

in $\sigma_{xx} + \sigma_{yy} (+\sigma_{zz}) = 1$. For d-dimensional systems under isotropic pressure, it is convenient to choose isotropic pressure, i.e. $\sigma_{xx} = \sigma_{yy} (= \sigma_{zz}) = 1/d$. However, Vlugt and van Eerd [38] used a different constraint $\sigma_{xx} + \sigma_{yy} = 1$ instead. With the latter constraint, small anisotropic pressure fluctuations occur.

We used Monte Carlo simulations in the force network ensemble to study the contact force distribution for the frictionless (unsheared) triangular lattice for both isotropic and anisotropic pressure. We also unravel the effect of the system size N for both constraints. Our results are summarised in Figure 1. The contact force distributions
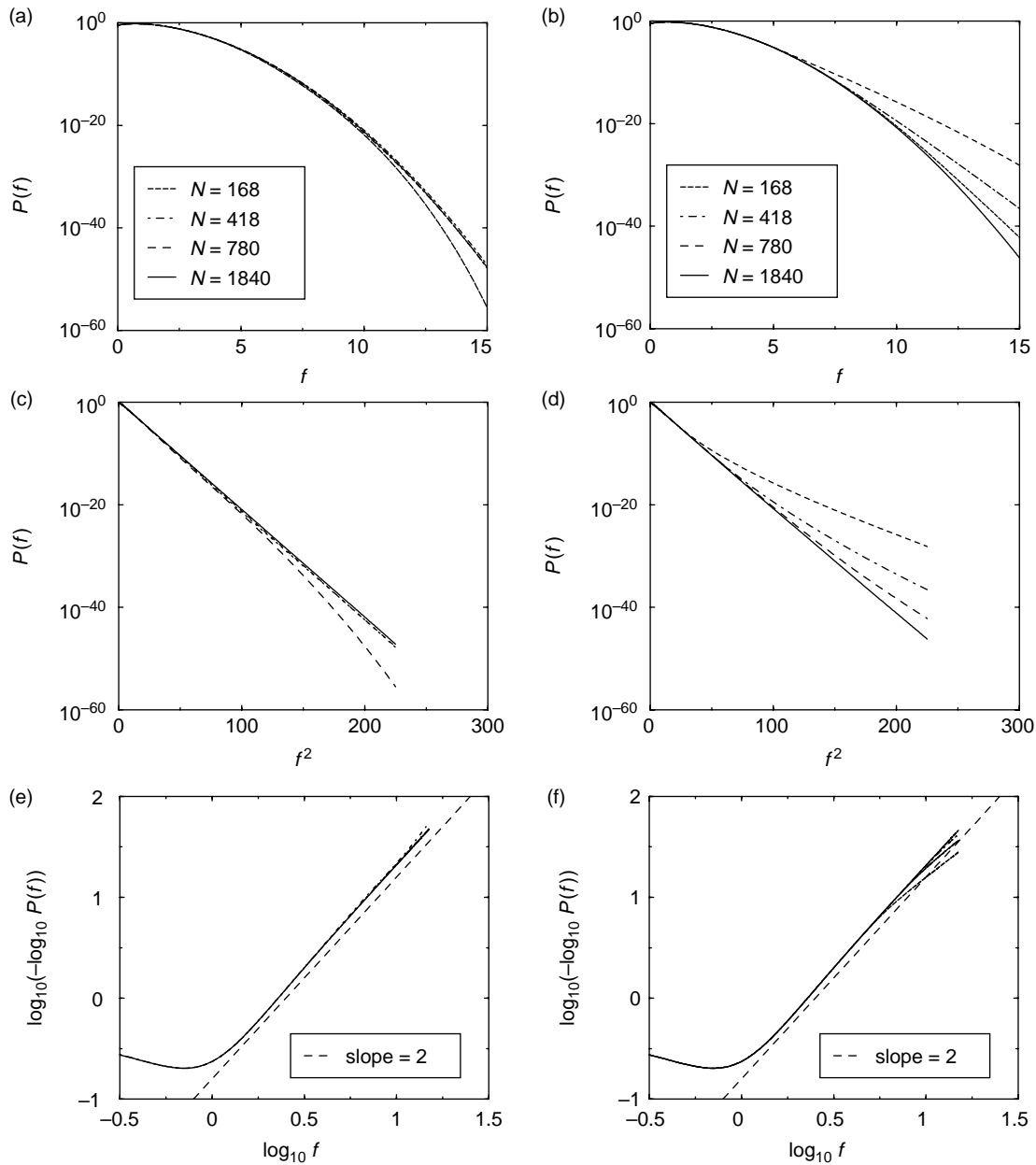
Figure 1. Contact force distribution $P(f)$ as a function of the system size (number of particles N) for the frictionless triangular lattice. (a,c,e) The constraint $\sigma_{xx} = \sigma_{yy} = 1/2$ is used. (b,d,f) The constraint $\sigma_{xx} + \sigma_{yy} = 1$ is used. In all simulations, $\sigma_{xy} = \sigma_{yx} = 0$.

that are calculated with $\sigma_{xx} = \sigma_{yy} = 1/2$ show no differences at forces below $f = 5$, but a finite-size effect is observed for larger forces, converging to a Gaussian distribution. The contact force distributions calculated with the anisotropic constraint $\sigma_{xx} + \sigma_{yy} = 1$ converges to the same Gaussian distribution, but the finite-size effect is much larger. The reason for this is that for small systems the fluctuations of σ_{xx} and σ_{yy} around 1/2 are quite large. For larger systems, these fluctuations become smaller, so eventually $\sigma_{xx} \approx 1/2$ and $\sigma_{yy} \approx 1/2$. Surprisingly, for small system sizes ($N = 168$), $P(f)$ shows an exponential decay when anisotropic pressure fluctuations are allowed. Note that the packings of this size are typically used in experiments.

3.2 Angle-resolved P(f)

Contact force distributions of sheared packings do not show a single characteristic feature, because shear stress induces force anisotropy that yields a variation in $\langle f \rangle$ depending on the orientation of the contact [35,39]. In good approximation, the average normal contact force along direction ϕ (Figure 2) can be described by

$$\bar{f}_n(\phi) = 1 + 2\tau\sin(2\phi) - b_2\cos(4\phi), \qquad (15)$$

with $\int d\phi \bar{f}_n(\phi) / \int d\phi = 1$ [35,48]. The parameter b_2 increases with increasing shear stress $\tau = \sigma_{xy}/\sigma_{xx}$ and by definition $b_2 = 0$ for $\tau = 0$. The second term in Equation (15) has the largest contribution to the force anisotropy. The 'total' $P(f)$ is a superposition over all the orientations of ϕ. Here, we numerically study the angle-resolved contact force distribution $P(f, \phi)$ by umbrella sampling. To accurately compute the tail of this distribution, separate simulations are needed for each ϕ, using the maximum contact force along the direction ϕ as an order parameter. The following symmetry applies to our system: $P(f, 45° - \phi) = P(f, 45° + \phi)$ and $P(f, 225° - \phi) = P(f, 225° + \phi)$. This has been used to improve sampling statistics.

A triangular lattice contains contact forces in three distinct orientations: (1) 0° and 180°, (2) 60° and 240°, and (3) 120° and 300°. In Figure 3, the contact force distributions are shown for these three orientations.
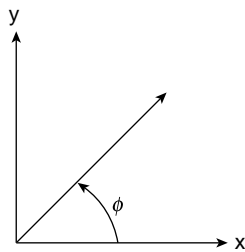

Figure 2. The angle ϕ in the used reference frame.

We see that for $\tau = 0$ all orientations have the same Gaussian decay of $P(f, \phi)$. The small differences in Figure 3(a) can be attributed to finite-size effects induced by periodic boundary conditions. If the system experiences shear stress ($\tau > 0$), the tails of the contact force distributions are still Gaussian, but as expected we observe a different slope in the linear-log plots; the probability of large contact forces oriented close to the direction of the shear stress (60° and 240°) becomes larger, while the probability of large contact forces oriented almost perpendicular to the direction of the shear stress (120° and 300°) becomes significantly smaller.

To study the angle-resolved $P(f, \phi)$ for 2D disordered systems, we constructed a histogram of all the contact forces in which the contact forces are grouped according to their orientation ϕ, see Figure 4. In Figure 5, the average contact force for each orientation is plotted in a polar diagram. Without shear stress, the average contact force equals one in all directions. With shear stress ($\tau > 0$), the average contact force in the direction of the shear stress (label 1 in Figure 4) becomes larger and the average force oriented almost perpendicular to this direction (label 6) becomes smaller (see Figure 5(a)). The orientation dependence of the average force is given in good approximation by Equation (15), see Figure 5(d). We also show a polar diagram for frictional particles as a function of shear stress (see Figure 5(b)) and as a function of the friction coefficient μ (see Figure 5(c)). From the latter figure we can conclude that force anisotropy decreases if we allow friction.

Figure 6 shows the angle-resolved $P(f, \phi)$ for disordered systems with frictionless particles. We see that the $P(f, \phi)$'s for systems experiencing shear stress decay at least as fast as a Gaussian. Certainly, the decay of the angle-resolved contact force distribution decays significantly faster than an exponential. This means that the (partly) exponential decay of the *total* $P(f)$ as was found by van Eerd et al. [39] is a direct result of averaging $P(f, \phi)$ over all ϕ, and not a result of exponential statistics of individual contact forces.

We also studied the angle-resolved contact force distribution for a fcc lattice experiencing shear stress. This lattice is oriented so that the close-packed planes lie in the xy-plane and are stacked along the z-axis. Contact forces in the fcc lattice have six distinct orientations, as shown in Figure 7. Shear stress of the form $\sigma_{xy} \neq 0$ and $\sigma_{yz} = \sigma_{xz} = 0$ is applied and we refer to the parameter $\tau = \sigma_{xy}/\sigma_{xx}$ as the shear stress. The stress direction is in the xy-plane at 45° with the x-axis. Figure 8 shows the direction-resolved $P(f)$ for a fcc lattice. All $P(f)$ decay as $a\exp[-bf^\alpha]$ with $\alpha \approx 1.7$, just as for unsheared disordered systems in 3D [39]. Similar to the triangular lattice, for different directions, we observe a different slope in the linear-log plots. Shear stress has the largest effect on the forces oriented in directions 2 and 3 as both
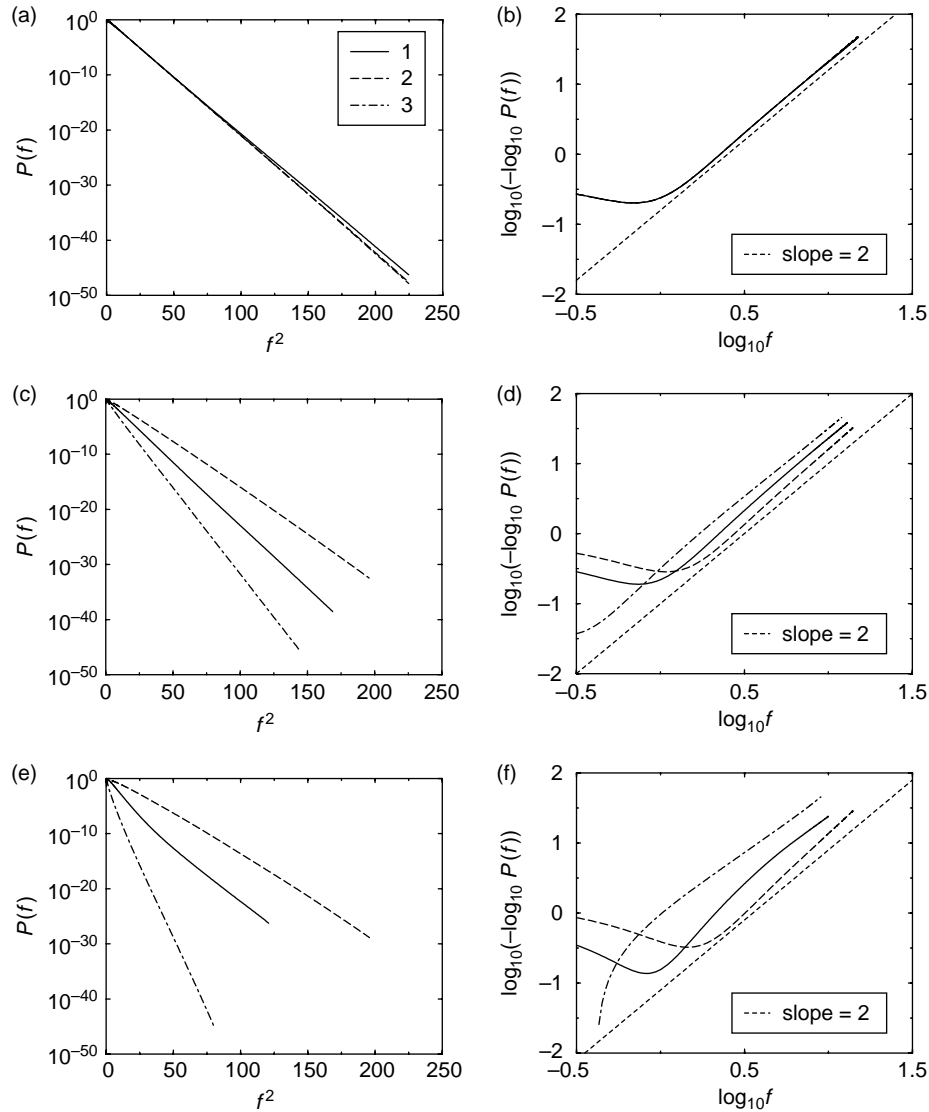
Figure 3. Angle-resolved contact force distributions for the frictionless triangular lattice ($N = 1840$ particles) with $\tau = 0$ (a,b), $\tau = 0.2$ (c,d) and $\tau = 0.4$ (e,f). The contact forces are oriented in three directions: (1) 0° and 180°, (2) 60° and 240°, and (3) 120° and 300°. If systems experience shear stress, the distribution $P(f, \phi)$ becomes different in the three given directions. For a fixed ϕ, $P(f)$ shows a Gaussian decay. In all simulations, $\sigma_{xx} = \sigma_{yy} = 1/2$.

are in the *xy*-plane along the direction of the shear stress. Forces not oriented in this plane (e.g. 5) are less affected.

3.3 Maximum possible force inside a packing

van Eerd et al. [39] have observed that for disordered packings in 2D, finite-size effects occur for the contact force distribution $P(f)$, especially for low-coordination numbers (z). One would observe such finite-size effects for contact forces close to the maximum contact force that a certain packing can sustain. When the maximum contact force of a packing ($f_{max}(\mathbf{f})$) is close to the maximum contact force that a certain packing can sustain, $P(f)$ will

show a very sharp decrease. Eventually, for very large f, $P(f)$ will decrease to zero for any packing [29].

In principle, conventional umbrella sampling [45] can be used to determine the maximum possible f_{max}. However, a huge number of iterations will be necessary as $P(f)$ will become extremely small close to the maximum possible f_{max}. To efficiently compute the maximum possible f_{max} for a given packing, we use the central idea of the recently proposed random-walk algorithm of Wang and Landau [49,50]. In this scheme, a random walk is performed in the space of all possible force networks $\mathbf{f}$. The simulation is started by setting a certain function $\lambda(f_{max}) = 1$ for all f_{max}. Starting from a particular
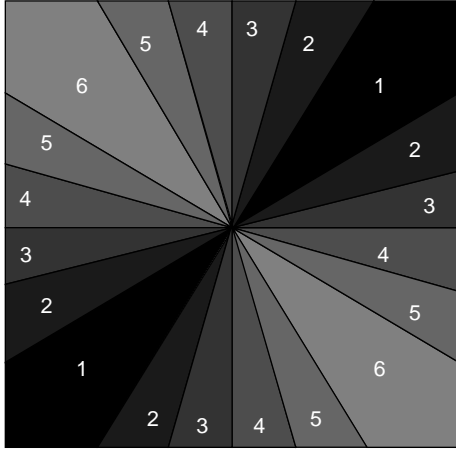
Figure 4. Diagram showing the different orientation segments for which the contact forces are evaluated. Note that the symmetries $P(f, 45° − \phi) = P(f, 45° + \phi)$ and $P(f, 225° − \phi) = P(f, 225° + \phi)$ are compatible with the symmetry of simple shear.

solution $\mathbf{f} = \mathbf{f}_0$, we perform a Monte Carlo scheme to sample all possible force networks. Trial moves that result in a configuration for which all $f_{n,ij} \geq 0$ are accepted with a probability

$$P_{acc}(o \rightarrow n) = \min\left(1, \frac{\lambda(f_{max}(o))}{\lambda(f_{max}(n))}\right) \qquad (16)$$

in which o and n are used to denote the old and new configurations, respectively. The crucial difference with conventional Monte Carlo simulations is that each time a force network with a certain f_{max} is visited, $\lambda(f_{max})$ is updated as follows: $\lambda(f_{max}) \rightarrow \lambda(f_{max}) \times m$ in which $m > 1$. This means that this scheme does not obey detailed balance. After many trial moves, eventually all possible values of f_{max} will be visited with (approximately) equal probability. From this, the maximum possible contact force of a certain contact network can be estimated. In the original version algorithm [49,50], the parameter m is slowly decreased from 2 to $1 + \delta$ (typically $\delta \approx 10^{-9}$) in a controlled way, such that
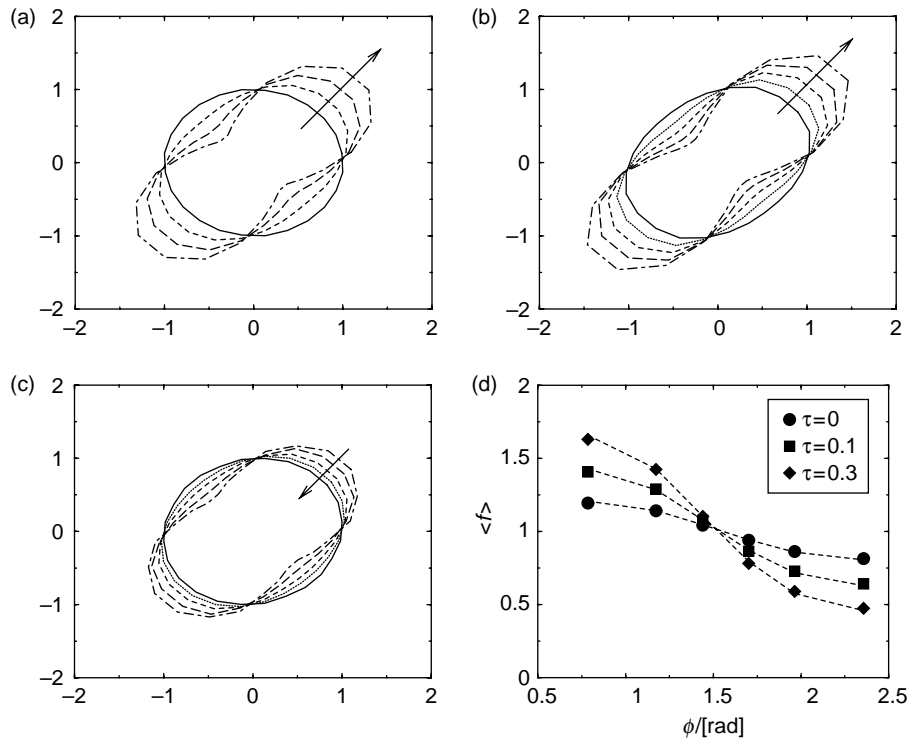

Figure 5. Polar diagrams of the average contact force per histogram segment for a two-dimensional disordered system with $N = 1024$ and $z = 5.5$. We have used the segments represented in Figure 4. In all simulations, $\sigma_{xx} = \sigma_{yy} = 1/2$. (a) Average contact force for frictionless particles as a function of the shear stress τ. The direction of the arrow indicates increasing τ: 0, 0.1, 0.2, 0.3. (b) Average contact force for frictional particles ($\mu = 0.5$) as a function of the shear stress τ. The direction of the arrow indicates increasing τ: 0.1, 0.2, 0.3, 0.4, 0.49. (c) Average contact force for frictional particles experiencing shear stress ($\tau = 0.2$) as a function of the the friction coefficient μ. The direction of the arrow indicates increasing μ: 0.1, 0.5, 1.0, 2.0, 10.0. (d) Average contact force for the system in (a) as a function of the angle ϕ. The dashed lines show a fit to Equation (15). The fitted values for b_2 are: 0.00652 ($\tau = 0.1$), 0.0288 ($\tau = 0.2$) and 0.0582 ($\tau = 0.3$).
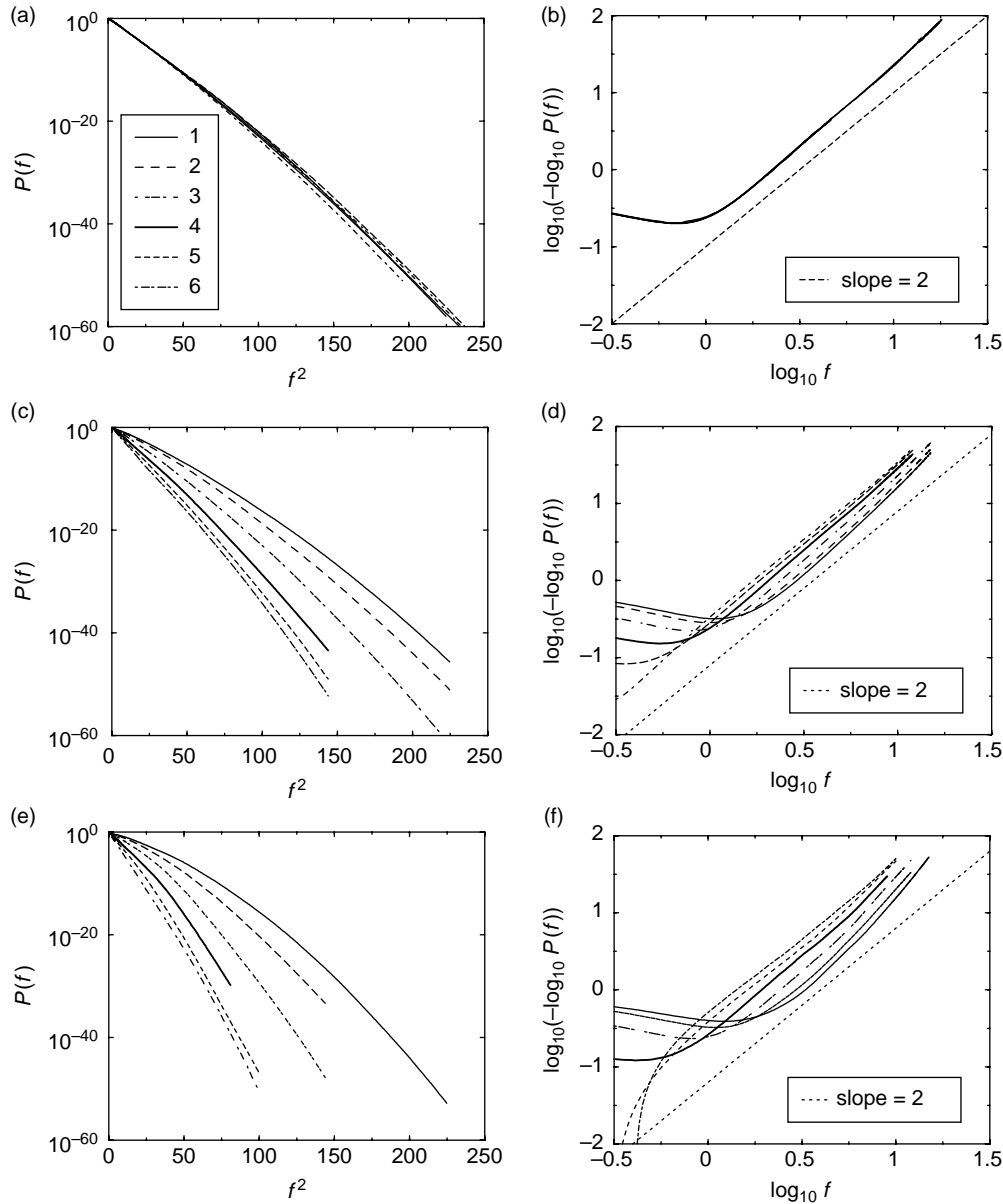
Figure 6. Angle-resolved contact force distributions of a two-dimensional frictionless disordered system ($N = 1024$, $z = 5.5$), divided in six directions. The numbers correspond to the segments in Figure 4. (a,b) $\tau = 0.0$, (c,d) $\tau = 0.2$, (e,f) $\tau = 0.3$. In all simulations, $\sigma_{xx} = \sigma_{yy} = 1/2$.

eventually configurations are sampled with a probability inversely proportional to the density of states. In our case, we are only interested in the maximum possible force that a packing can sustain and therefore we can safely set $m = 2$.

Figure 9(a) shows the computed maximum possible contact force in 2D disordered frictionless systems. Indeed, the maximum possible contact force increases with N and strongly depends on the coordination number z. This figure shows that relatively small systems are sufficient to study the statistics of large contact forces of typically $10\langle f \rangle$. In Figure 9(b), the corresponding $P(f)$

along with the maximum possible contact force is shown for $z = 4.5$. This figure shows strong evidence that the finite-size effects obtained in $P(f)$ are due to the fact that the maximum possible contact force of a small system with low z is quite small. Figures 9 and 10 suggest that finite-size effects in 3D are much smaller.

3.4 Maximum shear stress of a packing

To understand the relationship between the maximum shear stress τ_m and the coordination number z of a certain packing, we investigated the volume of the phase space
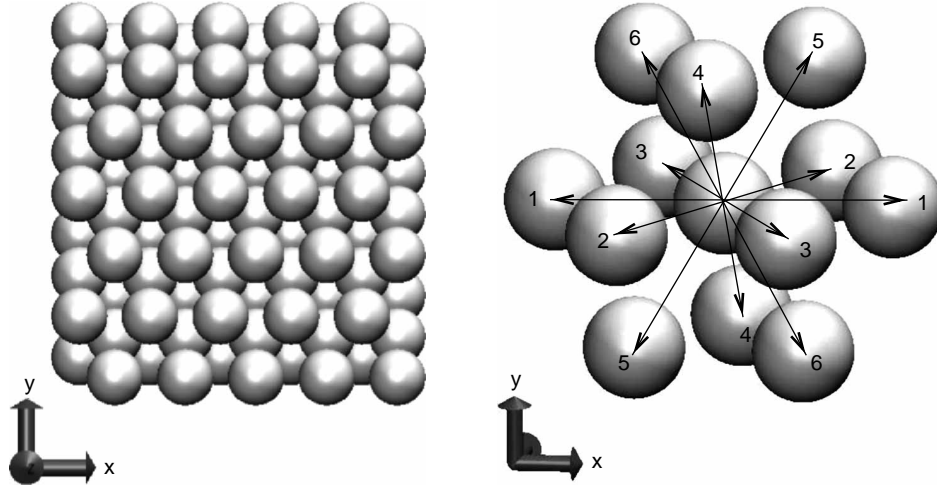
Figure 7. (left) Orthographic projection of an fcc lattice along the *z*-axis. The close-packed planes lie in the *xy*-plane and are stacked along the *z*-axis. The orientation becomes important if the system experiences shear stress. (right) Part of the fcc lattice in which the six distinct orientations of contacts between the particles are shown.

of allowed force networks. Snoeijer et al. [35] showed that for 2D frictionless systems this volume shrinks for increasing τ. The point at which the phase space volume is zero (τ_m) can be considered as a measure for the yield stress of the material. Ellenbroek and Snoeijer [48] predicted that the effect of friction on τ_m is quite small:

$$\tau_m = \frac{1 + \sqrt{1 + 3\mu^2}}{3}. \qquad (17)$$

This equation is valid for disordered 2D systems in the limit of $z \rightarrow 6$. To estimate the accessible volume of the space of all allowed force networks corresponding to a certain shear stress τ, we have used the following approaches:

- An effective linear measure for the size of the force space is the Euclidean distance L:

$$L(\tau) \equiv \sqrt{\left\langle \sum_{ij} (f_{n,ij} - f'_{n,ij})^2 \right\rangle}. \qquad (18)$$

The brackets denote an average over independent force network with normal forces $f_{n,ij}$ and $f'_{n,ij}$. Close to τ_m, $L(\tau)$ will show a sharp decrease.

- Direct calculation of the volume using umbrella sampling. The accessible volume $V(\tau)$ corresponding to a certain τ is proportional to the probability $P(\tau)$ measured in the force network ensemble in which the constraint on σ_{xy} has been removed. The dimension of the null space of this modified ensemble is one higher than that given in Table 1. Essentially, $P(\tau) = V(\tau)/V_{tot}$ in which $V_{tot} = \int_0^\infty d\tau V(\tau)$.

In principle, $P(\tau)$ and $L(\tau)$ will depend on the system size N and the nature of the packing. First, we study the Euclidean distance L as a measure for the volume of the phase space. Figure 11 shows the Euclidean distance $L(\tau)/L(\tau = 0)$ for 2D disordered systems ($N = 1024$) without and with friction ($\mu = 0.5$ and 1.0). The data are well described by

$$\frac{L(\tau)}{L(0)} = \sqrt{1 - \left(\frac{\tau}{\tau_m}\right)^\alpha}, \qquad (19)$$

in which τ_m and α are fitted. For frictionless systems, $\alpha \approx 2$ while frictional systems have a larger value for α. The obtained results for τ_m are summarised in Table 2. Our simulation results for frictional and frictionless systems are in excellent agreement with the prediction of Snoeijer et al. [35], which can be considered as an upper limit and therefore valid for large z. For $\tau < 0.2$, the Euclidean distance of frictional packings is almost constant, suggesting that small shear stress has a negligible influence on the normal contact forces.

In Figure 12, $P(\tau)/P(\tau = 0)$ is plotted as a function of τ for 2D disordered systems ($N = 1024$) without friction and with friction ($\mu = 0.5$ and 1.0). Already for small τ (i.e. far away from τ_m), $P(\tau)/P(\tau = 0)$ becomes extremely small. This means that, within the framework of the force network ensemble, packings do not spontaneously develop a shear stress. Computing $P(\tau)$ beyond $\tau = 0.2$ is very difficult and requires very long simulations, even if more overlapping windows are used in the umbrella sampling simulations. For frictionless systems, $P(\tau)/P(\tau = 0)$ strongly depends on the coordination number z, while this effect is not present for frictional systems. The latter observation is not surprising, as $L(\tau)$ of frictional systems is almost flat for $\tau < 0.2$.
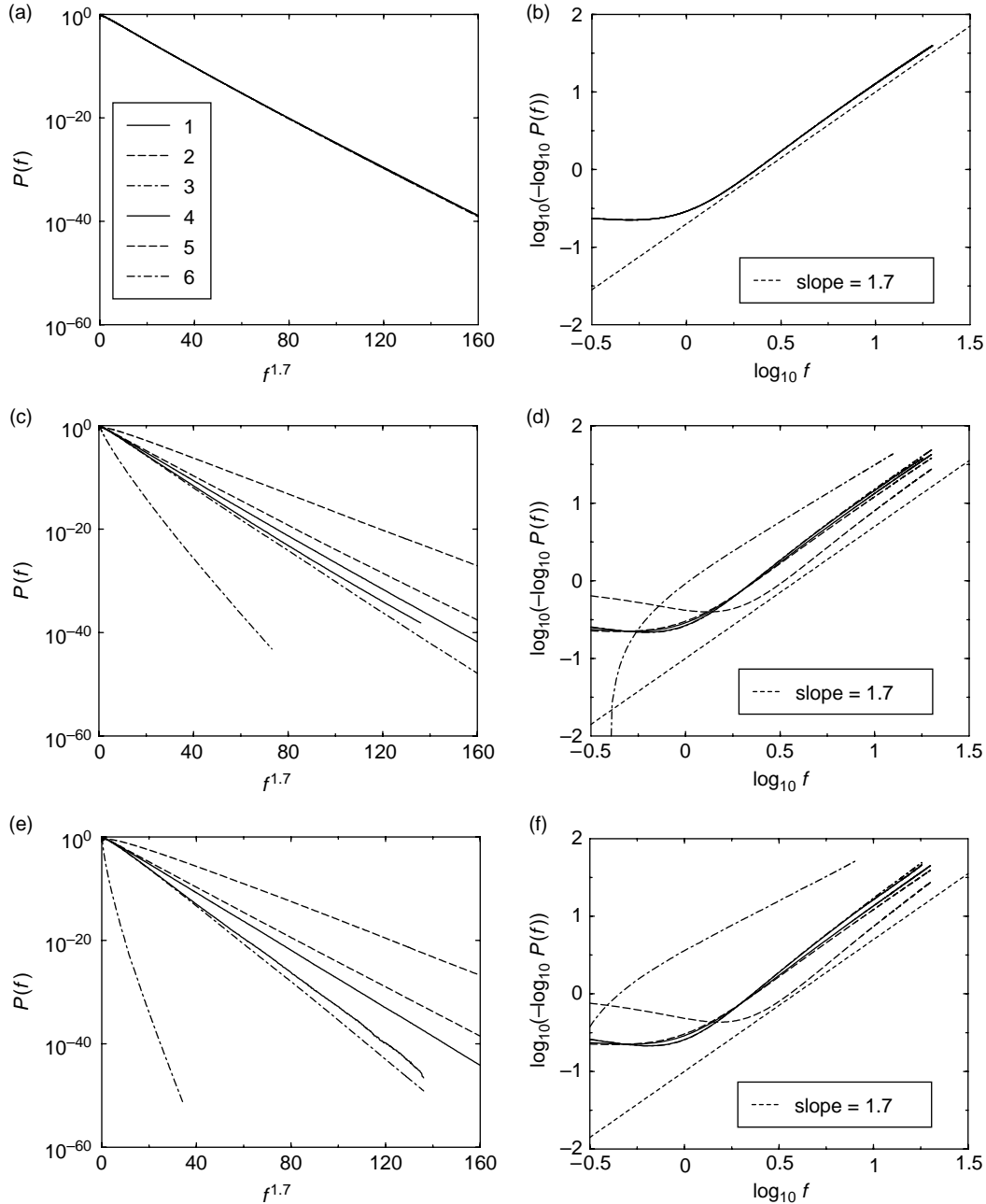
Figure 8. Direction-resolved contact force distributions of a three-dimensional crystalline system (fcc, $N = 7140$), divided in six orientations (see Figure 7). Shear stress τ is defined as $\sigma_{xy}/\sigma_{\alpha\alpha}$ with $\alpha = x, y, z$. (a,b) $\tau = 0$, (c,d) $\tau = 0.3$ and (e,f) $\tau = 0.39$. In all simulations, $\sigma_{xx} = \sigma_{yy} = \sigma_{zz} = 1/3$.

3.5 Wall versus bulk forces

Experimental measurements of contact forces at the boundaries (walls) show convincing exponential contact force distributions [11,51], while a stronger exponential decay is observed in many experimental [52,53] and computational studies [24,25] of bulk force statistics. The observed exponential force distributions have often been attributed to 'Boltzmann' type arguments; however,

Tighe et al. [40] have shown that the presence of additional *local* constraints, namely local force balance, leads to an additional *global* constraint that must be respected. It is this additional constraint that leads to Gaussian tails in $P(f)$. Because boundary grains have qualitatively different local environments from grains in the bulk, it is reasonable to ask whether this leads to differences in the statistics of forces at a wall.
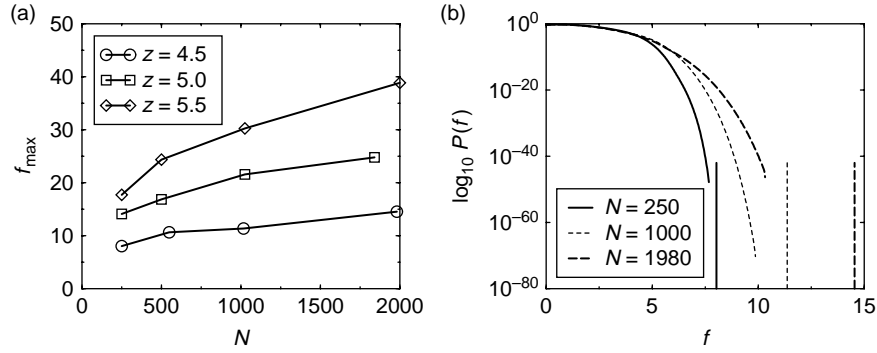
Figure 9. (a) The maximum possible contact force in unsheared networks of two-dimensional disordered frictionless systems for a different number of particles (N). (b) $P(f)$ for 2D disordered frictionless systems with $z = 4.5$. The vertical lines show the maximum possible contact force. In all simulations, $\sigma_{xx} = \sigma_{yy} = 1/2$.

A simple model for a system with wall and bulk forces is the so-called snooker triangle first studied by Snoeijer [41], see Figure 13. The stress on the system is controlled by constraining the sum of the wall forces for each of the three walls. All contact forces are repulsive and we will not consider friction. For $N = 3$ and 6 balls, it is possible to derive analytical solutions for the bulk and wall force statistics ($P(f_b)$ and $P(f_w)$, respectively) in the framework of the force network ensemble. For larger N, $P(f_b)$ and $P(f_w)$ have been computed by Snoeijer et al. [29]. However, the authors of this study were not able to make conclusive statements about the nature of the tail of these distributions.

We have re-examined the force distribution for snooker packings using umbrella sampling, see Figure 14. The distributions $P(f_b)$ and $P(f_w)$ have been normalised such that $\langle f_b \rangle = 1$ and $\langle f_w \rangle = 1$. The results unambiguously show that for large N both the bulk and wall forces have a Gaussian tail. It is not surprising that for large N, $P(f_b)$ approaches the contact force distribution of a triangular

lattice, which is known to have a Gaussian tail. Without the presence of local force balance on the balls near the wall, we would have exactly recovered the 'Boltzmann' argument resulting in an exponential distribution of wall forces. Apparently, the distribution of wall forces is changed significantly by the presence of bulk forces and local force balance constraints.

3.6 Contact force distributions for systems with 'real' interactions

Until now we studied contact force distributions in the framework of the force network ensemble. In this ensemble, the contact forces between particles are stochastic variables subject to various constraints (i.e. force balance on each grain, only repulsive contact forces, and a prescribed stress tensor) and do not originate from an interaction potential. It is interesting to investigate to what extent the contact force statistics of the force network ensemble is identical to that of forces derived from 'real' interactions, i.e. interactions that follow from an interaction (pair) potential.

Two cases are worth studying. First, the contact force distribution of the unconstrained 'real' system and second the contact force distribution of the 'real' system with the constraint of a zero net force on each particle. We shall refer to the latter systems as force balanced packings.

We first discuss force balanced packings of interacting particles. We expect that the contact force distribution is close to the one obtained in the force network ensemble. Molecular simulations of force balanced packings of interacting particles are non-trivial as one needs to include constraints on the net force on each particle, while the other cannot control the contact forces directly. Starting from random configurations of particles at very low density, we used a compression scheme to generate a large number of these packings with equal pressure P [47]. We studied 2D packings of $N = 2000$ bidisperse particles with
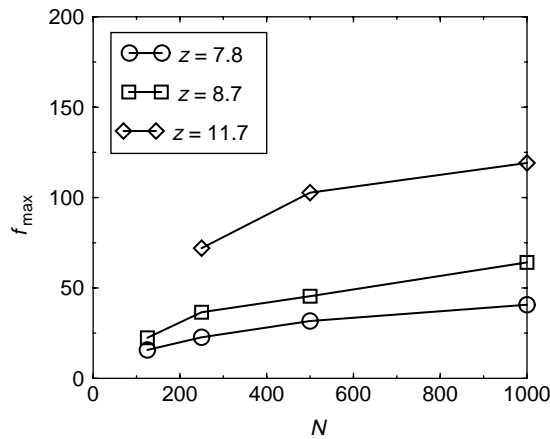

Figure 10. The maximum possible contact force in unsheared networks of three-dimensional disordered frictionless systems with a different number of particles (N). $\sigma_{xx} = \sigma_{yy} = \sigma_{zz} = 1/3$.
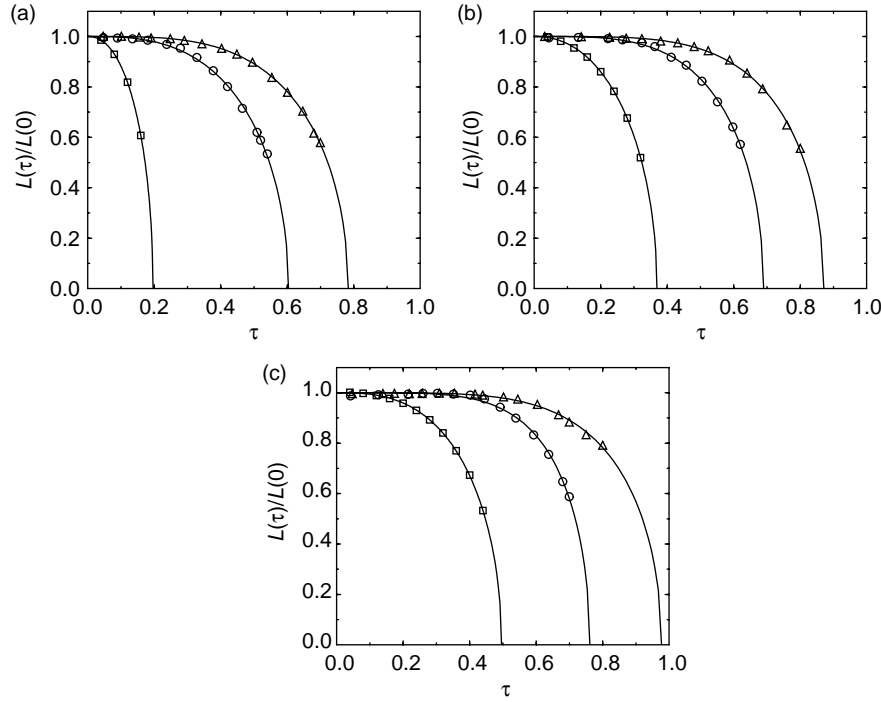
Figure 11. Euclidean distance $L(\tau)/L(\tau = 0)$ as a function of τ for 2D disordered systems with $N = 1024$ and (a) $z = 4.5$, (b) $z = 5.0$ (c) $z = 5.5$. The symbols are simulation data points and the solid lines are fits to Equation (19): no friction (square), $\mu = 0.5$ (circle) and $\mu = 1.0$ (triangle). In all simulations, $\sigma_{xx} = \sigma_{yy} = 1/2$.

diameter σ_i (50%/50% mixture, size ratio 1.4) interacting with either a WCA potential [54]

$$u_{\text{WCA}}(r_{ij}) = \begin{cases} u_{\text{LJ}}(r_{ij}) + \epsilon, & r_{ij} \leq 2^{1/6}\sigma_{ij} \\ 0, & r_{ij} > 2^{1/6}\sigma_{ij}, \end{cases} \quad (20)$$

or an harmonic potential (corresponding to linear springs)

$$u_{\text{HARM}}(r_{ij}) = \begin{cases} \epsilon(\sigma_{ij} - r_{ij})^2, & r_{ij} \leq \sigma_{ij} \\ 0, & r_{ij} > \sigma_{ij}, \end{cases} \quad (21)$$

where $\sigma_{ij} = (\sigma_i + \sigma_j)/2$ and ϵ is an energy parameter. The Lennard-Jones potential u_{LJ} is defined as

$$u_{\text{LJ}}(r_{ij}) = 4\epsilon\left[\left(\frac{\sigma}{r_{ij}}\right)^{12} - \left(\frac{\sigma}{r_{ij}}\right)^6\right]. \quad (22)$$

Table 2. The maximum shear stress τ_m for disordered systems with coordination number z and $N = 1024$ particles obtained by fitting Equation (19) to the simulation data in Figure 11. Included is also the prediction according to Equation (17).

	$z = 4.5$	$z = 5.0$	$z = 5.5$	Equation (17)
No friction	0.20	0.37	0.50	0.67
$\mu = 0.5$	0.60	0.69	0.76	0.77
$\mu = 1.0$	0.78	0.87	0.98	1.00

Figure 15 shows the contact force distributions and the coordination numbers for force balanced packings with pressure P consisting of particles that interact with a harmonic potential. In the same figure, we also show $P(f)$ for a frictionless triangular lattice in the force network ensemble. The distributions for the 'real' interactions are obtained from averaging over 4000 force balanced packings for each pressure. The average coordination number z strongly depends on the applied pressure. In the limit of small pressure, the coordination number approaches the isostatic limit $z_c = 4$. For all simulations, we have verified that the system is sufficiently far from z_c so that the simulations do not suffer from a lack of self-averaging [26,55]. The contact force distribution for a triangular lattice in the force network ensemble is close to $P(f)$ for the 'real' interactions at dimensionless pressure $P \approx 0.03$. Both distributions have a Gaussian tail. For larger pressures (and larger z), the contact force distribution bends down faster than a Gaussian. The observation of a Gaussian tail is in agreement with the simulations of O'Hern et al. [25,55]. These authors also presented an argument based on equilibrium systems to predict the decay of the large force tail, resulting in a Gaussian tail for harmonic potentials and a nearly exponential tail for a WCA potential. It is important to note that the systems of Figure 15 are *not* in thermodynamic equilibrium so the argument may not apply.
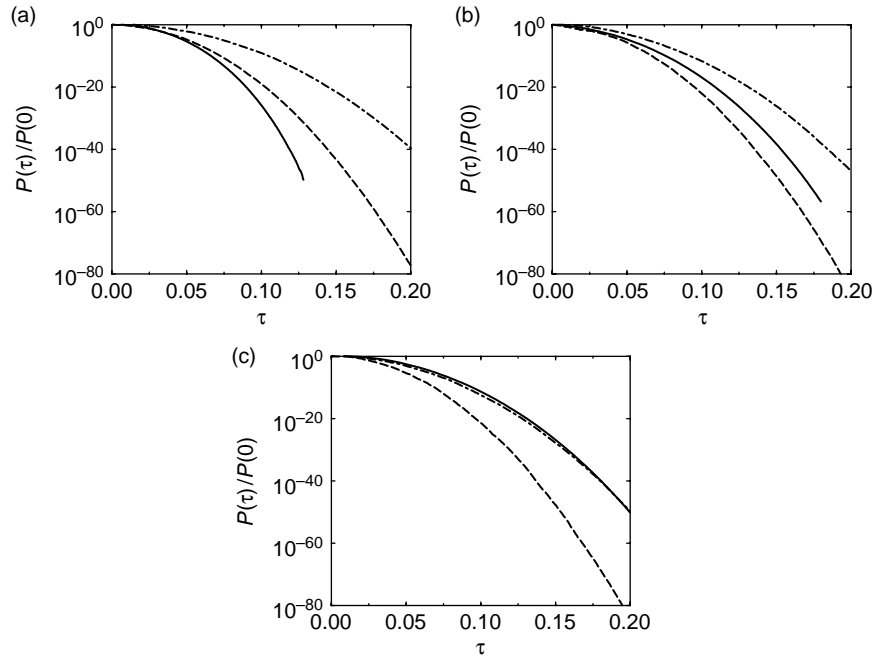
Figure 12. $P(\tau)/P(\tau = 0)$ against τ for 2D disordered systems $N = 1024$: no friction (solid), $\mu = 0.5$ (long dashed) and $\mu = 1.0$ (dot-dashed). (a) $z = 4.5$, (b) $z = 5.0$ and (c) $z = 5.5$. In all simulations, $\sigma_{xx} = \sigma_{yy} = 1/2$.

To investigate the effect of the interaction potential, we have studied force balanced packings of particles interacting with a WCA potential. The equilibrium prediction for the WCA interaction potential gives a tail of $P(f) \sim \exp[-af^{12/13}]$, i.e. qualitatively different from the case of the harmonic potential. We have investigated the effect of the pressure P as well as the hardness κ of the interaction potential:

$$\kappa = \frac{\langle f \rangle}{\langle r_{ij} \rangle} \left\langle \frac{\partial f}{\partial r_{ij}} \right\rangle^{-1}. \quad (23)$$

Particles that are harder have a lower value of κ. The value of κ can be controlled directly by changing the energy parameter ϵ of the WCA potential, while keeping the pressure P constant. Figure 16(a) shows that the systems with the same κ have the same coordination number z, and we have verified that they also have the same contact force distribution. Analogous to what we found for a harmonic interaction, we find that the contact force distribution for a triangular lattice in the force network ensemble is close to $P(f)$ for energy parameter $\epsilon \approx 16$ and dimensionless pressure $P = 15$. Again, they both have a Gaussian tail. In fact, all distributions of Figure 16(d) have a Gaussian tail. Our results suggest that force statistics in ensembles of static packings are independent of the interaction potential, contrary to thermal arguments and in agreement with one of the postulates of the force network ensemble.

Next, we turn to the case of the force distribution of an unconstrained 'real' system. These systems do *not* have force balance. Tighe et al. [40] have shown that local force balance determines the decay of the contact force distribution. Figure 17 shows the contact force distribution of particles interacting with a WCA potential simulated at a finite temperature T. The glass transition temperature of this system is $k_B T_g/\epsilon \approx 1.1$. Clearly, $P(f)$ decays
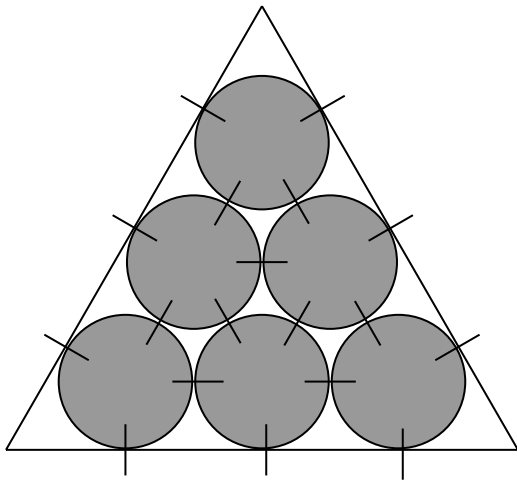

Figure 13. Snooker triangle of $N = 6$ balls with nine forces between the balls (bulk forces) and nine forces between a ball and the wall (wall forces). The stress on the system is controlled by constraining the sum of the wall forces for each of the three walls. Note that particles at the wall have five contacts, while particles in the bulk have six contacts.
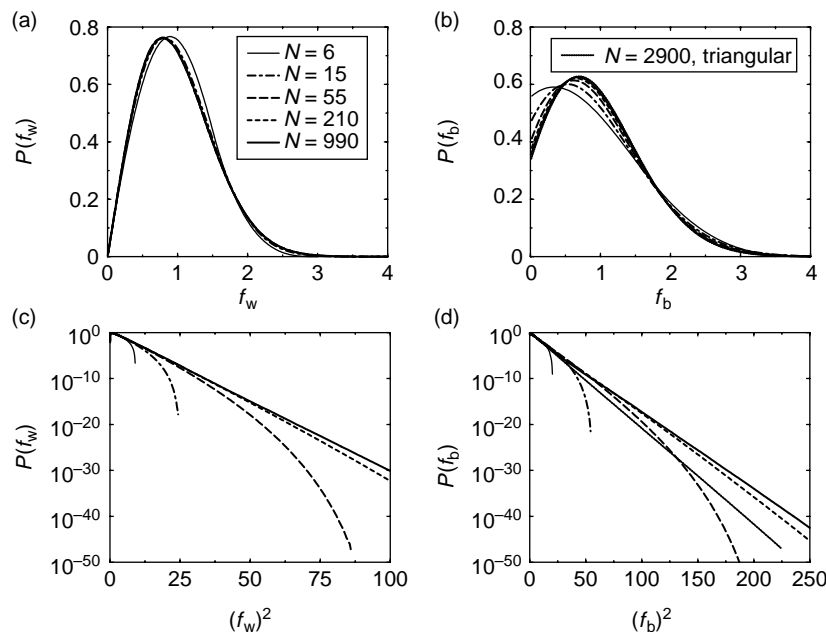
Figure 14. Contact force distribution for wall forces (a,c) and bulk forces (b,d) for snooker packings of several sizes. $P(f_w)$ and $P(f_b)$ have been normalised such that $\langle f_b \rangle = 1$ and $\langle f_w \rangle = 1$. For comparison, we also show $P(f)$ for a frictionless triangular lattice in (b,d).
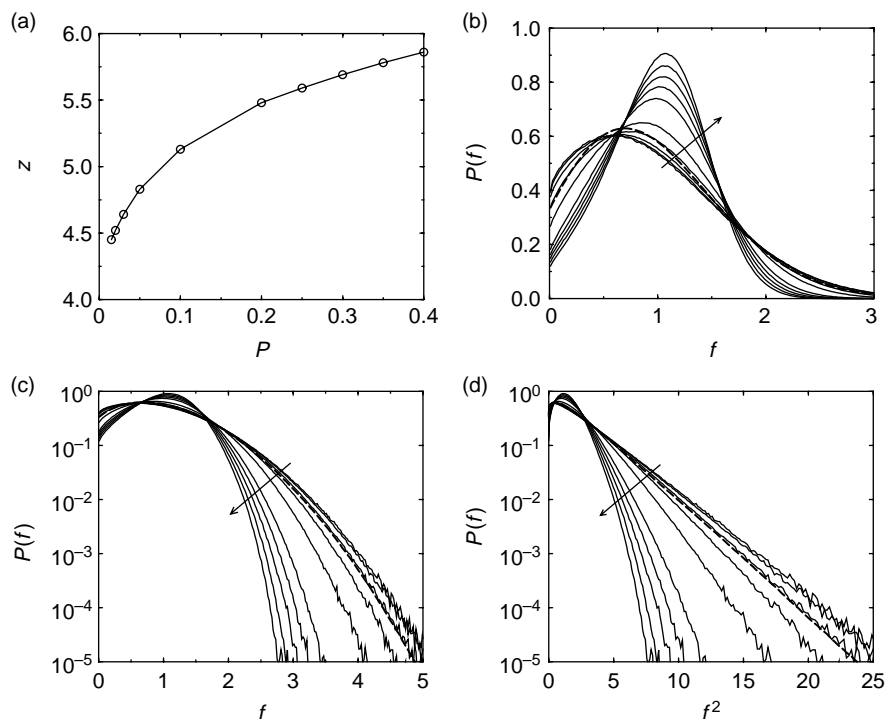

Figure 15. (a) The coordination number z as a function of the pressure P resulting from simulations of systems with particles interacting via the harmonic potential ($\epsilon/k_B T = 1$). (b,c,d) Contact force distribution of systems with particles interacting via the harmonic potential ($\epsilon/k_B T = 1$). The same data are plotted using different axes. The direction of the arrow indicates increasing pressure P (in dimensionless units 0.015, 0.02, 0.03, 0.05, 0.1, 0.2, 0.25, 0.3, 0.35, 0.4). For comparison, we also show $P(f)$ for a triangular lattice in the force network ensemble (dashed curve).
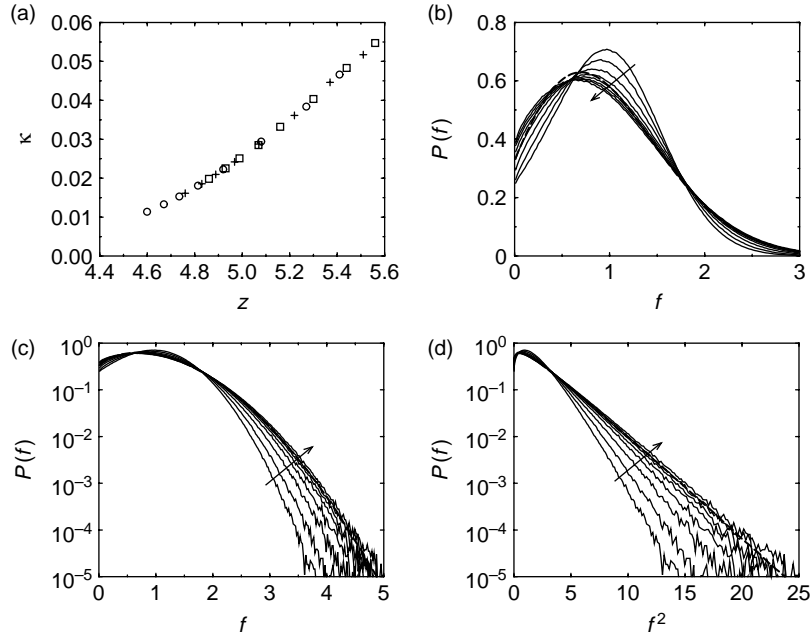
Figure 16. (a) The hardness κ as a function of the coordination z. The data points are results from simulations of systems with particles interacting via the WCA potential and dimensionless pressure $P = 15$ (circle), $P = 25$ (plus) and $P = 35$ (square). (b,c,d) Contact force distribution of systems with particles interacting via the WCA potential and pressure $P = 15$. The direction of the arrow indicates increasing energy parameter ϵ/k_BT (1, 2, 4, 7, 10, 13, 16, 20) and decreasing κ (0.0466, 0.0384, 0.0294, 0.02227, 0.01810, 0.01531, 0.01331, 0.01138). For comparison, we also show $P(f)$ for a triangular lattice in the force network ensemble (dashed curve).

exponentially both for $T > T_g$ and $T < T_g$, in agreement with previous molecular dynamics simulations [25]. Note that, despite the accuracy of our data, it is not possible to distinguish the predicted tail for thermally equilibrated
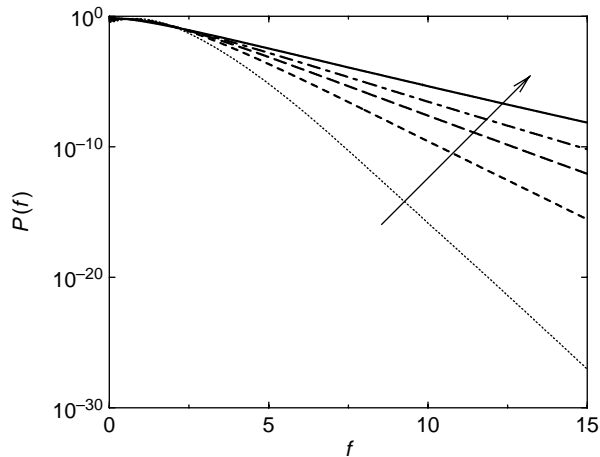

Figure 17. Contact force distributions of a two-dimensional system ($N = 1024$, $\rho = N/V = 0.747$) with a WCA potential *without* force balance as a function of the temperature. The direction of the arrow indicates increasing k_BT/ϵ: 0.2, 0.4, 0.6, 0.8, 1.2. These simulations have been obtained using umbrella sampling where we have assumed local equilibrium. We have verified that MD simulations of the same system using a constraint temperature lead to identical results.

packings, $\exp[-af^{12/13}]$, from a simple exponential. In any case, this is qualitatively different from the Gaussian tails of the contact force distribution that we found for the constrained 'real' interactions, and strikingly reinforces the conclusion that the presence of local force balance alter the tail of $P(f)$. If we revisit the arguments of Tighe et al. [40] and remove the additional global constraint that results from local force balance, we find a Boltzmann-like tail, i.e. $P(f) \sim \exp[-af]$. This naive extrapolation neglects the question of when conventional equilibrium statistical mechanics should be abandoned for, i.e. stress-based ensembles of the sort described by Tighe et al. [40], a question which is beyond the scope of this work.

4. Conclusions

We showed that in the force network ensemble, in the presence of shear stress the contact force distribution $P(f)$ is strongly direction dependent. As a result the tail of the orientation-averaged $P(f)$ may look (partly) exponential even though for each individual direction the tail is Gaussian. We developed a method to find the maximum possible contact force in a system and showed that this maximum possible contact force strongly increases for increasing system size. In the force network ensemble, the wall-contact force distribution may differ essentially from the bulk-contact force distribution. However, for snooker packings we found that both distributions have a Gaussian

decay. Finally, we made a detailed comparison between $P(f)$ in the force network ensemble and $P(f)$ from molecular simulations of particles with a 'real' pair interaction. We show that these distributions are different in general. Nevertheless, our calculations suggest that applying the constraint of local mechanical equilibrium, the contact force distribution of the 'real' system crosses over towards the distribution of the force network ensemble.

Acknowledgement

References

[1] L.K.A. Dorren, *A review of rockfall mechanics and modelling approaches*, Prog. Phys. Geogr. 27 (2003), pp. 69–87.

[2] S. De Toni and P. Scotton, *Two-dimensional mathematical and numerical model for the dynamics of granular avalanches*, Cold Regions Sci. Technol. 43 (2005), pp. 36–48.

[3] W.R. Ketterhagen, J.S. Curtis, C.R. Wassgren, and B.C. Hancock, *Modeling granular segregation in flow from quasi-three-dimensional, wedge-shaped hoppers*, Powder Technol. 179 (2008), pp. 126–143.

[4] F.Y. Fraige, P.A. Langston, and G.Z. Chen, *Distinct element modelling of cubic particle packing and flow*, Powder Technol. 186 (2008), pp. 224–240.

[5] E. DesRosiers Lachiver, N. Abatzoglou, L. Cartilier, and J.S. Simard, *Agglomeration tendency in dry pharmaceutical granular systems*, Eur. J. Pharm. Biopharm. 64 (2006), pp. 193–199.

[6] K. Lee, T. Kim, P. Rajniak, and T. Matsoukas, *Compositional distributions in multicomponent aggregation*, Chem. Eng. Sci. 63 (2008), pp. 1293–1303.

[7] M. van Hecke, *Shape matters*, Science 317 (2007), pp. 49–50.

[8] M. van Hecke, *Granular matter: a tale of tails*, Science 435 (2005), pp. 1041–1042.

[9] H.P. Zhu, Z.Y. Zhou, R.Y. Yang, and A.B. Yu, *Discrete particle simulation of particulate systems: theoretical developments*, Chem. Eng. Sci. 62 (2007), pp. 3378–3396.

[10] H.M. Jaeger, S.R. Nagel, and R.P. Behringer, *Granular solids, liquids, and gases*, Rev. Mod. Phys. 68 (1996), pp. 1259–1273.

[11] C.-h. Liu, A.R. Nagel, D.A. Schecter, S.N. Coppersmith, S. Majumdar, O. Narayan, and T.A. Witten, *Force fluctuations in bead packs*, Science 269 (1995), pp. 513–515.

[12] D.M. Mueth, H.M. Jaeger, and S.R. Nagel, *Force distribution in a granular medium*, Phys. Rev. E 57 (1998), pp. 3164–3169.

[13] D.L. Blair, N.W. Mueggenburg, A.H. Marshall, H.M. Jaeger, and S.R. Nagel, *Force distributions in three-dimensional granular assemblies: effects of packing order and interparticle friction*, Phys. Rev. E 63 (2001), 041304.

[14] J.M. Erikson, N.W. Mueggenburg, H.M. Jaeger, and S.R. Nagel, *Force distributions in three-dimensional compressible granular packs*, Phys. Rev. E 66 (2002), 040301.

[15] G. Løvoll, K.J. Måløy, and E.G. Flekkøy, *Force measurements on static granular materials*, Phys. Rev. E 60 (1999), pp. 5872–5878.

[16] T.S. Majmudar and R.P. Behringer, *Contact force measurements and stress-induced anisotropy in granular materials*, Nature 435 (2005), pp. 1079–1082.

[17] N.P. Kruyt and L. Rothenburg, *Probability density functions of contact forces for cohesionless frictional granular materials*, Int. J. Solids Struct. 39 (2002), pp. 571–583.

[18] P.T. Metzger, *Granular contact force density of states and entropy in a modified Edwards ensemble*, Phys. Rev. E 70 (2004), 051303.

[19] P.T. Metzger, *H theorem for contact forces in granular materials*, Phys. Rev. E 77 (2008), 011307.

[20] P.T. Metzger and C.M. Donahue, *Elegance of disordered granular packings: a validation of Edward's hypothesis*, Phys. Rev. Lett. 94 (2005), 148001.

[21] A.H.W. Ngan, *Mechanical analog of temperature for the description of force distribution in static granular packings*, Phys. Rev. E 68 (2003), 011301.

[22] S. Henkes, C.S. O'Hern, and B. Chakraborty, *Entropy and temperature of a static granular assembly: an* ab initio *approach*, Phys. Rev. Lett. 99 (2007), 038002.

[23] H.A. Makse, D.L. Johnson, and L.M. Schwartz, *Packing of compressible granular materials*, Phys. Rev. Lett. 84 (2000), pp. 4160–4163.

[24] F. Radjai, M. Jean, J.J. Moreau, and S. Roux, *Force distributions in dense two-dimensional granular systems*, Phys. Rev. Lett. 77 (1996), pp. 274–277.

[25] C.S. O'Hern, S.A. Langer, A.J. Liu, and S.R. Nagel, *Force distributions near jamming and glass transitions*, Phys. Rev. Lett. 86 (2001), pp. 111–114.

[26] C.S. O'Hern, L.E. Silbert, A.J. Liu, and S.R. Nagel, *Jamming at zero temperature and zero applied stress: the epitome of disorder*, Phys. Rev. E 68 (2003), 011306.

[27] L.E. Silbert, G.S. Grest, and J.W. Landry, *Statistics of the contact network in frictional and frictionless granular matter*, Phys. Rev. E 66 (2002), 061303.

[28] J.H. Snoeijer, T.J.H. Vlugt, M. van Hecke, and W. van Saarloos, *Force network ensemble: a new approach to static granular matter*, Phys. Rev. Lett. 92 (2004), 054302.

[29] J.H. Snoeijer, T.J.H. Vlugt, W.G. Ellenbroek, M. van Hecke, and J.M.J. van Leeuwen, *Ensemble theory for force networks in hyperstatic granular matter*, Phys. Rev. E 70 (2004), 061306.

[30] S.F. Edwards and R.B.S. Oakeshott, *Theory of powders*, Physica A 157 (1989), pp. 1080–1090.

[31] T. Unger, J. Kertész, and D.E. Wolf, *Force indeterminacy in the jammed state of hard disks*, Phys. Rev. Lett. 94 (2005), 178001.

[32] B.P. Tighe, J.E.S. Socolar, D.G. Schaeffer, W.G. Mitchener, and M.L. Huber, *Force distributions in a triangular lattice of rigid bars*, Phys. Rev. E 72 (2005), 031306.

[33] S. Ostojic and D. Panja, *Elasticity from the force network ensemble in granular media*, Phys. Rev. Lett. 97 (2006), 208001.

[34] S. McNamara and H. Herrmann, *Measurement of indeterminacy in packings of perfectly rigid disks*, Phys. Rev. E 70 (2004), 061303.

[35] J.H. Snoeijer, W.G. Ellenbroek, T.J.H. Vlugt, and M. van Hecke, *Sheared force-networks: anisotropies, yielding and geometry*, Phys. Rev. Lett. 96 (2006), 098001.

[36] S. Ostojic, E. Somfai, and B. Nienhuis, *Scale invariance and universality of force networks in static granular matter*, Nature 439 (2006), pp. 828–830.

[37] S. Ostojic, *Statistical mechanics of static granular matter*, Ph.D. thesis, University of Amsterdam, Amsterdam, The Netherlands, 2006.

[38] T.J.H. Vlugt and A.R.T. van Eerd, *Krachtenbalans op zandkorrels*, Vakidioot, Studievereniging A-Eskwadraat 1 (2005), pp. 19–23.

[39] A.R.T. van Eerd, W.G. Ellenbroek, M. van Hecke, J.H. Snoeijer, and T.J.H. Vlugt, *The tail of the contact force distribution in static granular materials*, Phys. Rev. E 75 (2007), 060302 (R).

[40] B.P. Tighe, A.R.T. van Eerd, and T.J.H. Vlugt, *Entropy maximization in the force network ensemble for granular solids*, Phys. Rev. Lett. 100 (2008), 238001.

[41] J.H. Snoeijer, *Statistics of force networks in granular media*, Ph.D. thesis, Leiden University, Leiden, The Netherlands, 2003.

[42] W.H. Press, S.A. Teukolsky, W.T. Vertterling, and B.P. Flannery, *Numerical Recipes in Fortran 77: The Art of Scientific Computing*, 2nd ed., Cambridge University Press, Cambridge, 1992.

[43] M.P. Allen and D.J. Tildesley, *Computer Simulations of Liquids*, Oxford University Press, Oxford, 1987.

[44] S. Ostojic, T.J.H. Vlugt, and B. Nienhuis, *Universal anisotropy in force networks under shear*, Phys. Rev. E 45 (2007), 030301 (R).

[45] D. Frenkel and B. Smit, *Understanding Molecular Simulation: From Algorithms to Applications*, 2nd ed., Academic Press, San Diego, 2002.

[46] G.M. Torrie and J.P. Valleau, *Nonphysical sampling distributions in Monte Carlo free-energy estimation: umbrella sampling*, J. Comp. Phys. 23 (1977), pp. 187–199.

[47] A.R.T. van Eerd, *Statistics of large contact forces in granular matter*, Ph.D. thesis, Utrecht University, Utrecht, The Netherlands, 2008.

[48] W.G. Ellenbroek and J.H. Snoeijer, *Bounds on the yield stress of cohesionless granular matter*, J. Stat. Mech. (2007), P01023.

[49] F. Wang and D.P. Landau, *Efficient, multiple-range random walk algorithm to calculate the density of states*, Phys. Rev. Lett. 86 (2001), pp. 2050–2053.

[50] F. Wang and D.P. Landau, *Determining the density of states for classical statistical models; A random walk algorithm to produce a flat histogram*, Phys. Rev. E 64 (2001), p. 56101.

[51] E.I. Corwin, H.M. Jaeger, and S.R. Nagel, *Structural signature of jamming in granular media*, Nature 435 (2005), pp. 1075–1078.

[52] J. Brujić, S.F. Edwards, I. Hopkinson, and H.A. Makse, *Measuring the distribution of interdroplet forces in a compressed emulsion system*, Physica A 327 (2003), p. 201.

[53] J. Zhou, S. Long, Q. Wang, and A.D. Dinsmore, *Measurement of forces inside a three-dimensional pile of frictionless droplets*, Science 312 (2006), pp. 1631–1633.

[54] J.D. Weeks, D. Chandler, and H.C. Andersen, *Role of repulsive forces in determining the equilibrium structure of simple liquids*, J. Chem. Phys. 54 (1971), pp. 5237–5247.

[55] C.S. O'Hern, S.A. Langer, A.J. Liu, and S.R. Nagel, *Random packings of frictionless particles*, Phys. Rev. Lett. 88 (2002), 075507.